Topology Optimization of Skeleton-reinforced Soft Pneumatic Actuators for Desired Motions

Shitong Chen, Feifei Chen, *Member, IEEE,* Zizheng Cao, Yusheng Wang, Yunpeng Miao, Guoying Gu, *Member, IEEE,* and Xiangyang Zhu, *Member, IEEE*

***Abstract*—Multimaterials with different modulus can endow soft robots with embodied intelligence that deliver spatially-varying deformation upon actuation. There is an increasing need for design tools that can rigorously and efficiently generate material layouts for desired motions. Here, we present a design paradigm for soft pneumatic multimaterial actuators by attaching a stiffer material layer as skeleton to softer inflated rubber, and develop a topology optimization based framework to automatically generate the skeleton layout that leads the actuator to achieve desired motions such as bending or twisting. Our method is enabled by a dynamic level set function to describe and track the topological change of the skeleton, large-deformation analysis compatible with the varying skeleton layout, and a gradient-based optimizer to govern the evolution of material layout, with the geometric and material nonlinearities taken into account. A forward geometric mapping and a backward design velocity mapping are constructed to allow manipulating the level sets on the planar space. We show that the design methodology is capable of generating high-performance bending and twisting actuators of cylindrical or customized cone shape. The simulation and experiment results show that, the bending actuator achieves a free bending angle 73°and blocking force 2.05 N, and the twisting actuator achieves a large rotation angle of 143°.**

***Index Terms*—Soft robots, soft pneumatic actuators, topology optimization, multimaterial design.**

I. Introduction

In the past decade, the use of soft materials for building robots has enabled a new generation of robots with unprecedented flexibility, generally referred to as soft robots. The inherent distributed compliance offered by freeform geometry and material diversity are imbuing soft bodies with programmable mechanical properties to deliver desired complex motion behaviors under physical stimuli. This embodied mechanical intelligence has allowed for various innovative applications, and in the meantime requires fundamentally new design perspectives [1].

The motion behavior of a soft body is concurrently determined by its geometry, material, and actuation, and these factors are usually physically coupled. This is the case for pneumatic actuators where the pressure loading is directly related to the channel shape, known as design dependent loads. Spatially gradient materials are promising to create complex motion behaviors that may be hard to achieve using a single material, and usually leads to simple geometry and compact bodies in applications such as actuators [2], end-effectors [3] and jumping robots [4]. The complex interplay among multiple materials, geometry profiles, and external actuations in a highly nonlinear physical process makes the design of soft actuators and robots with desired deformations extremely difficult. Designers usually have to rely on intuitions or experiences, and a mathematical approach to automate the design process is in high demand.

Mechanical modeling of soft multimaterial systems has shed light on the design optimization. Fiber-reinforced elastomers for constructing pneumatic actuators provided excellent examples in which the elastomers are typically isotropic, while the anisotropic fibers offer an avenue for exploring the deformation mode of the actuator including extension, contraction, bending, and twisting [5]–[7]. Connolly *et al.* developed an analytical model to identify the fiber arrangements for tracking a desired kinematic trajectory [8]. However, this mechanical model can only describe regular layouts of fibers and thus is not applicable to general multimaterial design of soft robots.

To explore the vast design space of soft actuators, researchers have investigated topology optimization of the freeform material layout, driven by cables [9]–[11], electric fields [12] or magnetic fields [13]. Among them, topology optimization for soft pneumatic robots has been of great interest due to their wide use. Ma *et al.* made an initial attempt by modeling soft pneumatic materials with a fixed frame and then optimizing the material densities of the frame to generate desired motions [14], but the fixed frame does not allow amorphous topological change. Chen *et al.* designed a pneumatic bending actuator by optimizing internal cavities with topological change [15], and found that the optimized channel presents similar geometric features with Pneu-Nets design [16]. Instead of relying on varying the cavity geometry that involves cumbersome design-dependent loads, Zhang *et al.* optimized the reinforced material placed on a soft pneumatic tube to produce desired bending motions [17].

We summarize the representative works on design of soft pneumatic actuators and robots in Table I, with a special focus on the design methodology, and it is found that the initial attempts on topology optimization of soft pneumatic robots all rely on linear optimization models [15], [17]. However, this assumption of linearity is insufficient to capture the physical complex behaviors of highly deformable soft materials. The large deformation upon actuation typically induces significant

This work was supported by the National Natural Science Foundation of China (Grants 51905340 and 91948302), and was sponsored by Shanghai Sailing Program (19YF1422900). (*Corresponding author: Feifei Chen.*)

The authors are with State Key Laboratory of Mechanical System and Vibration, Shanghai Jiao Tong University, and Robotics Institute, School of Mechanical Engineering, Shanghai Jiao Tong University, Shanghai 200240, China (email: stonehot@sjtu.edu.cn; ffchen@sjtu.edu.cn; caozizheng@sjtu.edu.cn; gloomysheng@sjtu.edu.cn; mythmyp@sjtu.edu.cn; guguoying@sjtu.edu.cn; mexyzhu@sjtu.edu.cn).

TABLE I: Summary of current published works on design optimization of soft pneumatic robots.

Authors / Citation	Design Space	Mechanical Analysis	Optimization Algorithm	Application
Connolly *et al.* 2012 [8]	Fiber angle	Nonlinear	N/A	Bending, twisting actuators
Ma *et al.* 2017 [14]	Frame material density	Nonlinear	Gradient-based	Shape-matching
Chen *et al.* 2019 [15]	Topology of channel	Linear	Gradient-based	Bending actuator
Zhang *et al.* 2019 [17]	Partial topology of reinforced material	Linear	Gradient-based	Bending actuator
This work	Full topology of skeleton layer	Nonlinear	Gradient-based	Bending, twisting actuators

geometric nonlinearity, and the material hyperelasticity is dominant for large strains, necessitating a nonlinear stress-strain model. These nonlinearities are yet to be incorporated into the optimization model to fully exploit the potential of topology optimization for generative design of soft robots [1]. The paradigm shift in modeling and optimization translates into addressing the challenge of nonlinear large deformation analysis and sensitivity analysis in nonlinear regions throughout the optimization process.

In this paper, resting on an actuator design paradigm by attaching a stiffer material layer as skeleton to softer inflated rubber, we develop a design methodology to automatically generate the skeleton layout that leads the actuator to achieve desired motions such as bending and twisting. The pneumatic rubber embedded inside remains unchanged as the non-design domain so that the pressure loading is design-independent. The varying skeleton layout is described and tracked by a dynamic level set function, and we construct a forward geometric mapping from the planar regular design domain to the curved shape of the physical skeleton layer and a backward design velocity mapping, to allow manipulating the level sets on the planar space. Combined with the nonlinear deformation analysis of a design candidate, an adjoint sensitivity analysis was conducted to infer how the desired motion quantitatively depends on the skeleton profile, and thus the skeleton layout can evolve toward the steepest descent direction to generate the optimal design, without designer's intervention.

Our optimized design is validated through both simulation and experiments which agree well in both linear and nonlinear regions. We demonstrate that the consideration of nonlinearities delivers better design. Very interestingly, characteristic structural features abstracted from the optimized design are well explainable in terms of producing bending or twisting motions, which provides new inspiration for designers. The bending actuator prototype achieves a free bending angle 73°and blocking force 2.05 N, and the twisting actuator achieves a large rotation angle of 143°. To demonstrate the generality of our design method, we further extend the design domain to cone-shaped actuators for desired bending or twisting motions, and the simulation and experiment results well validate the effectiveness.

II. Geometry Model

A. Level Sets

The skeleton layer rests on a curved shape and is allowed to change in topology to deliver the optimal design. Level sets have been widely used in engineering applications for describing and tracking topological shapes [18], and have been well embedded in topology optimization methods [19]. Here, we construct level sets defined in a signed distance function whose zero contour represents the skeleton layout (see Fig. 1),

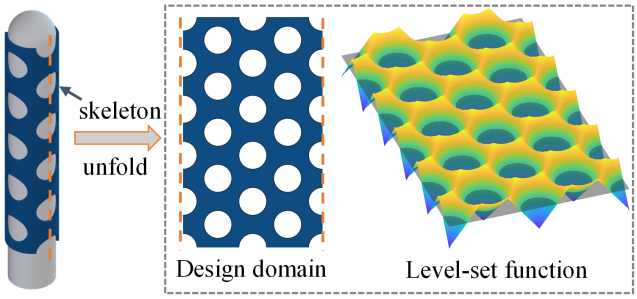

Fig. 1: Representation of a level set function to describe the skeleton layout.

$$\begin{cases} \phi(\mathbf{X},t) > 0\,, & \forall \mathbf{X} \in \Omega \\ \phi(\mathbf{X},t) = 0\,, & \forall \mathbf{X} \in \Gamma \\ \phi(\mathbf{X},t) < 0\,, & \forall \mathbf{X} \in \mathrm{D}/(\Omega \cup \Gamma) \end{cases} \tag{1}$$

where D denotes the unfolded rectangular design domain, Ω denotes the solid area of the skeleton, Γ denotes the boundaries, $\mathbf{X} \in \mathrm{D}$ represents the coordinates of a point in question, and t denotes pseudo-time for evolution. The evolution of skeleton layout translates into the variation of zero contour of the level set function, governed by the Hamilton-Jacobi equation,

$$\frac{\partial \phi(\mathbf{X},t)}{\partial t} = -|\nabla \phi(\mathbf{X},t)| V_n \tag{2}$$

where V_n refers to the normal velocity at point $\mathbf{X}$.

B. Domain Transformation

The curved shape the skeleton layer rests on can split into a rectangular as the design domain on which we define the level set function, and thus a geometry mapping is constructed. The forward mapping of a vector is constructed by $\mathbf{a}^c = \mathbf{J}\mathbf{a}^r$ with $\mathbf{a}^r$ and $\mathbf{a}^c$ vectors in 2D and 3D space, respectively, and $\mathbf{J}$ is the mapping matrix. The backward mapping of the moving velocity is

$$V_n^r = \mathbf{G}\mathbf{n}^c \cdot \mathbf{n}^r V_n^c \tag{3}$$

with V_n^r and V_n^c moving velocity in 2D and 3D space, respectively, $\mathbf{n}^r$ and $\mathbf{n}^c$ the normal directions in 2D and 3D surfaces, respectively, and $\mathbf{G}$ is the inverse mapping of $\mathbf{J}$. For a cylindrical skeleton layer, the mapping is isometric, leading to $V_n^r = V_n^c$.

C. Domain Connectivity

The connectivity issue of the skeleton geometry arises when it splits into the rectangular domain. Additional operations are needed to ensure the signed distance property and connectivity. Here, we construct an augmented level set function by periodically tessellating the original level set function to ensure the signed distance property on the cutting edge, and impose their interconnectivity by parameterization. Parameterization of level sets in B-splines provides a simple and fast way to weld and polish the edges by directly restricting the weight coefficients in B-splines [20]. We constrain the coefficients related to the cutting edges of the design domain to guarantee the connectivity of the level set function. The reader may refer to [20] for the technical details. In this work, to ensure the continuity of the design velocity which points to the boundary normal direction, C^1 boundary connectivity is imposed.

III. Optimal Design of Skeleton Layout

In this section, we will formulate the skeleton layout design as a topology optimization problem and develop a computational framework to automate the iterative optimization.

A. State Equation

When the actuator undergoes deformation, the induced displacement field $\mathbf{u}$ defines the deformation gradient by $\mathbf{F} = \mathbf{I} + \nabla\mathbf{u}$ with the gradient operator with respect to the reference domain and $\mathbf{I}$ the second-order identity tensor. We employ a hyperelastic model to characterize the material nonlinearity of silicone rubbers and linear elastic model to characterize the much stiffer material for the skeleton layer. Without loss of generality, the generalized neo-Hookean model [21] is adopted with the free energy density W expressed by,

$$W = \frac{\mu}{2}\Big(\frac{\mathrm{trace}(\mathbf{F}\cdot\mathbf{F}^{\mathrm{T}})}{J^{2/3}} - 3\Big) + \frac{\kappa}{2}(J-1)^2 \tag{4}$$

where μ and κ denote the initial shear modulus and bulk modulus, respectively, and $J = \det(\mathbf{F})$.

In the context of geometric nonlinearity, we employ the Green-Lagrange strain and the second Piola-Kirchhoff stress measures which are work-conjugate. The state equation can be derived based on principle of energy conservation,

$$a(\mathbf{u},\mathbf{v},\phi) = l(\mathbf{u},\mathbf{v}), \quad \forall\mathbf{v}\in U \tag{5}$$

with the variational structural form and load form

$$a(\mathbf{u},\mathbf{v},\phi) = \int_{\Omega_0^{\mathrm{s}}} \mathbf{s}(\mathbf{u}) : \bar{\mathbf{E}}(\mathbf{u},\mathbf{v})\mathrm{d}\Omega + \int_{\Omega_0^{\mathrm{r}}} \mathbf{s}(\mathbf{u}) : \bar{\mathbf{E}}(\mathbf{u},\mathbf{v})\mathrm{d}\Omega \tag{6}$$

$$l(\mathbf{u},\mathbf{v}) = p\int_{\Gamma_0^{\mathrm{r}}} \mathbf{v}\cdot\left(\mathbf{m}_{\mathrm{r}}\cdot\mathbf{F}^{-1}\right) J\mathrm{d}\Gamma \tag{7}$$

where $\mathbf{s}$ is the stress, $\Omega_0^{\mathrm{r}} \in \mathbb{R}^3$ is the undeformed region of soft rubber, $\Omega_0^{\mathrm{s}} \in \mathbb{R}^3$ is the undeformed skeleton layer, $\mathbf{v}$ is the virtual displacement field, U denotes the kinematically admissible space, $\mathbf{m}_{\mathrm{r}}$ is the normal vector to the surface, Γ_0^{r} is the inner surface, and p is the applied pressure. The variational Lagrange strain tensor is

$$\bar{\mathbf{E}}(\mathbf{u},\mathbf{v}) = \frac{1}{2}\left(\mathbf{F}^{\mathrm{T}}\cdot\nabla\mathbf{v} + \nabla\mathbf{v}^{\mathrm{T}}\cdot\mathbf{F}\right). \tag{8}$$

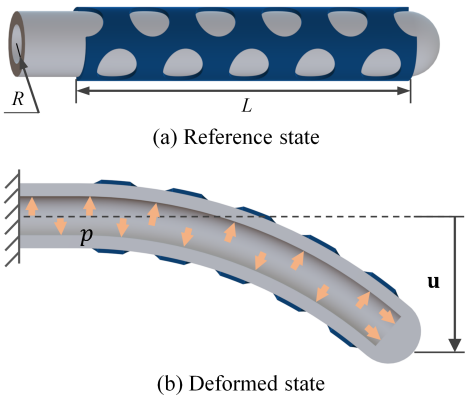

(a) Reference state

(b) Deformed state

Fig. 2: A skeleton-reinforced soft actuator for bending motion.

B. Optimization Model

The skeleton layout is optimized in order to produce as closely as possible the desired displacements. The topology optimization model is formulated by

$$\begin{aligned} \min_{\Omega} \quad & J_{\mathrm{obj}} = \frac{1}{2}\sum_{i\in A}\left\|\mathbf{u}_i - \mathbf{u}_i^{\mathrm{d}}\right\|^2 \\ \text{subject to} \quad & a(\mathbf{u},\mathbf{v}) - l(\mathbf{u},\mathbf{v}) = 0,\ \forall\mathbf{v}\in U, \\ & s_c - f|\mathrm{D}| = 0 \end{aligned} \tag{9}$$

where J_{obj} is the design objective, $\mathbf{u}^{\mathrm{d}}$ is the desired displacement field, A denotes the set of points of interest, $s_c = \int_{\Omega_0^{\mathrm{s}}}\mathrm{d}\Omega$ defines the skeleton volume, and the volume constraint plays regularization roles when performing optimization, with f and $|\mathrm{D}|$ the given volume fraction for the skeleton and the total volume of the design domain.

C. Sensitivity Analysis

To investigate how the desired motion quantitatively depends on the skeleton layout, we carry out sensitivity analysis with the adjoint method. The Lagrangian is formulated by

$$L = J_{\mathrm{obj}} + a(\mathbf{u},\mathbf{w},\phi) - l(\mathbf{u},\mathbf{w}) + \lambda\left(s_c - f|\mathrm{D}|\right) \tag{10}$$

where $\mathbf{w}\in U$ denotes the adjoint displacement field, and λ is the Lagrange multiplier for penalizing the constraint. The derivative of Lagrangian with respect to pseudo time is

$$\dot{J}_{\mathrm{obj}} = \sum_{i\in A}\left(\mathbf{u}_i - \mathbf{u}_i^{\mathrm{d}}\right)\dot{\mathbf{u}}_i \tag{11}$$

$$\begin{aligned} \dot{a}(\mathbf{u},\mathbf{w},\phi) = & \int_{\Omega_0^{\mathrm{s}}}\left[\dot{\mathbf{s}}(\mathbf{u}) : \bar{\mathbf{E}}(\mathbf{u},\mathbf{w}) + \mathbf{s}(\mathbf{u}) : \dot{\bar{\mathbf{E}}}(\mathbf{u},\mathbf{w})\right]\mathrm{d}\Omega \\ & + \int_{\Gamma_0^{\mathrm{s}}} \mathbf{s}(\mathbf{u}) : \bar{\mathbf{E}}(\mathbf{u},\mathbf{w})V_n\mathrm{d}\Omega \end{aligned} \tag{12}$$

$$\dot{l}(\mathbf{u},\mathbf{w}) = p\int_{\Gamma_0^{\mathrm{r}}}\left[\mathbf{w}\cdot(\mathbf{m}_{\mathrm{r}}\cdot\dot{\mathbf{F}}^{-1})J + \mathbf{w}\cdot(\mathbf{m}_{\mathrm{r}}\cdot\mathbf{F}^{-1})\dot{J}\right]\mathrm{d}\Gamma \tag{13}$$

$$\dot{s}_c = \int_{\Gamma_0^{\mathrm{s}}} V_n\mathrm{d}\Gamma \tag{14}$$

where Γ_0^{s} is the boundary of the skeleton. Without loss of generality, $\dot{\mathbf{w}}$ is set to be zero. Since $\dot{\mathbf{u}}$ is unknown, all terms

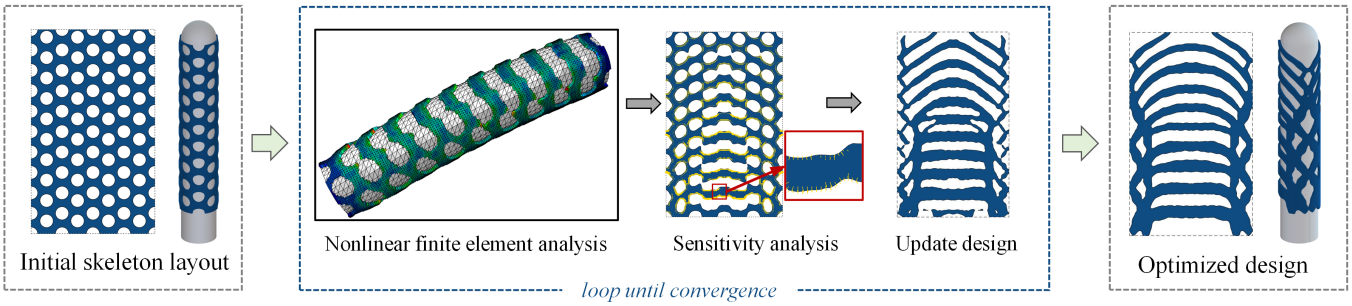

Fig. 3: Flowchart of designing the skeleton layout by topology optimization.

containing $\dot{\mathbf{u}}$ are collected and their sum is set to be zero by selecting a unique $\mathbf{w}$, which yields the so-called adjoint equation. After mathematical derivations, the adjoint equation numerically translates into a linear finite element equation

$$\mathbf{K}(\mathbf{u})\mathbf{w} = \mathbf{P} \tag{15}$$

with $\mathbf{K}$ the tangent stiffness matrix of the actuator which is function of the displacement field, and $\mathbf{P}$ is an assembled vector consisting of the magnitude of $\mathbf{u}^{\mathrm{d}} - \mathbf{u}$ at degrees of freedom of interest and zero otherwise. In this work, a bending actuator is designed and the maximal bending motion is pursued at the endpoint, i.e. $|\mathbf{u}^{\mathrm{d}}| = \infty$, in which case $\mathbf{P}$ is equivalently a unit concentrated load by noting that (15) is a linear equation. The adjoint displacement $\mathbf{w}$ is solved such that the terms containing $\dot{\mathbf{u}}$ are eliminated. Then the derivative of the Lagrangian $\dot{L}$ is rewritten by

$$\dot{L} = \int_{\Gamma_0^{\mathrm{s}}} \left[\mathbf{s}(\mathbf{u}) : \bar{\mathbf{E}}(\mathbf{u}, \mathbf{w}) + \lambda\right] V_n \mathrm{d}\Gamma \tag{16}$$

To this end, for ensuring the steepest descent direction, the normal velocities on the skeleton boundaries can be selected,

$$V_n(\mathbf{X}) = -\left[\mathbf{s}(\mathbf{u}) : \bar{\mathbf{E}}(\mathbf{u}, \mathbf{w}) + \lambda\right], \ \forall \mathbf{X} \in \Gamma_0^{\mathrm{s}}. \tag{17}$$

It can be observed from (15)-(17) that, the sensitivity and design velocity are function of the induced displacement field which is load-dependent, necessitating the consideration of the nonlinear physical deformation process.

D. Design Workflow

In the design workflow, the skeleton layout is iteratively renewed by optimization procedure, as shown in Fig. 3. The optimizer starts from an initial skeleton profile, followed by nonlinear finite element analysis to evaluate the deformation behavior of the actuator. The adjoint displacement is solved by (15). Thereafter, the sensitivity analysis is conducted to generate the design velocity field based on which the skeleton layout is updated by solving the Hamilton-Jacobian equation. The movement distance satisfies the Courant-Friedrichs-Lewy condition for numerical stability. The above process is repeated until the design candidate fulfills the predefined convergence criterion.

The volume constraint is set to be 0.5 during the optimization and is imposed by updating the Lagrange multiplier. We adopt the following updating strategy,

$$\lambda_{k+1} = \lambda_k + \xi_k(\varsigma_k - f|\mathrm{D}|), \xi_{k+1} = \gamma\xi_k, k = 1, 2, .., N_s \tag{18}$$

with ξ_k the penalization factor at the kth step, $\gamma \geq 1$ an expansion parameter and $N_s = 200$ the prescribed iteration limit. The optimization algorithm is terminated when the relative difference of the objective function values between two successive iterations becomes lower than 10^{-3}.

IV. Numerical Implementation

In this section, we will introduce how the large deformation analysis is addressed for the design candidates which may take amorphous shapes during the optimization process, and investigate how the geometric and material nonlinearities tailor the optimization results.

A. Large Deformation Analysis

For the nonlinear finite element analysis compatible with varying skeleton layouts, we customized an automatic numerical framework by connecting Matlab and Abaqus. We adopt shell elements (S3) to discretize the thin-wall skeleton layer and C3D4H elements (4-node linear tetrahedron and hybrid) for soft rubber. The numerical results show that shell elements have good interaction properties with the inner rubber part, leading to better convergence.

When calling Abaqus to perform analysis, a key issue is to coordinate varying level set descriptions and the finite element mesh in Abaqus. People usually keep the geometry unchanged and vary the material properties by interpolation, giving rise to artificial intermediate materials, as in [15], [17]. These artificial materials increase the node scale and the computation cost, and more importantly, the weak materials which represent voids are prone to suffering mesh distortions and then cause severe convergence issues. In this work, instead of relying on use of weak materials, we deactivate the shell elements corresponding to voids by evaluating the nodal level set function to obtain distinct skeleton layout, leading to greatly improved computational convergence and efficiency. Specifically, an element is deactivated when the mean of its nodal level-set function values is negative, expressed by

$$\sum_{N_i \in \Omega_e} \phi(N_i) < 0, \quad \text{for element } e \tag{19}$$

when Ω_e denotes the domain of element e. The generated shell mesh well reproduces the skeleton layout defined by zero contour of the level set function, and the boundary quality can be tuned by the resolution of the shell mesh.

This article has been accepted for publication in a future issue of this journal, but has not been fully edited. Content may change prior to final publication. Citation information: DOI 10.1109/TMECH.2021.3071394, IEEE/ASME Transactions on Mechatronics

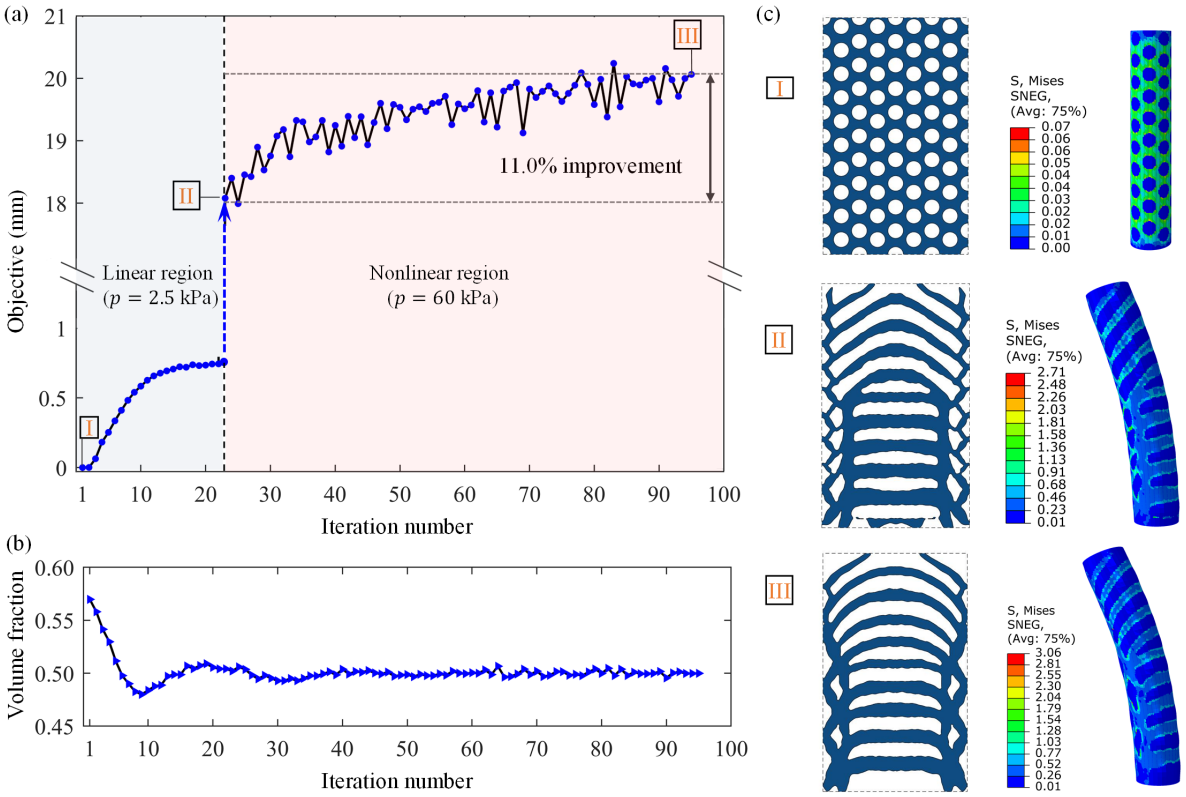

Fig. 4: Optimization results: history of (a) design objective and (b) volume fraction, and (c) three design candidates.

The geometry dimensions for analysis and experiments are specified here. The bending actuator is of length $L = 82.5$ mm, outer perimeter $2\pi R = 50$ mm. The skeleton layer is of uniform thickness 1 mm. The inner soft rubber tube is of uniform thickness 3.18 mm. The material properties for the inner soft rubber are: shear modulus μ =184 kPa and bulk modulus κ =18.35 MPa. Its Young's modulus at small strains is 0.55 MPa. The material properties for the skeleton are: Young's modulus 19.46 MPa, and Poisson's ratio 0.495. The reader may refer to Sec. V. A for details of material selection.

B. Gradually Loading Scheme

Considering the intermediate design candidates during optimization may easily suffer convergence issues, the applied pressure is gradually increased with the optimization iterations. This operation is similar to [22] in which the linear optimization result is taken as the starting point for the nonlinear optimization. At the first stage, the applied pressure is 2.5 kPa, the induced strain is small, and thus the actuator exhibits a linear response. The optimization conducted at this low pressure is referred to as the linear region, as shown in Fig. 4. When the optimization converges in the linear region, we increase the pressure to a high level, i.e. 60 kPa, and the optimization continues and leads to significant improvement up to 11.0% in terms of the concerned bending displacement. At high pressures, the actuator undergoes large deformation and exhibits considerable geometric and material nonlinearities which are well incorporated into the optimizer to further refine the skeleton layout during nonlinear regions.

C. Optimization Results

The evolving process of the skeleton layout is shown in Fig. 4. The optimization starts with an initial design which contains many small circles to allow for sufficient geometric flexibility for potential topological evolutions. The holes in the initial design merge into complex topological shapes that are hard to perceive by intuition. Three key states are shown in Fig. 4, including their bending configurations and the induced stress. Several key structural features are observed from the final optimized design, which are also well explainable. First, the circumferential bars well constrain the radical inflation. Second, as expected, more materials are distributed on the compressive part in order to induce bending, functioning as the limiting layer as in many pneumatic actuators [16]. Third, very interestingly, it is observed that the skeleton connection on the compressive side results in parallelogram shape which may function as a mechanism to transfer circumferential expansions into compression and further enhance bending motions, as suggested by [23]. This finding sheds light into the innovative design of the limiting layer.

The optimization is gradient-based and thus naturally depends on the initial guess. Therefore, we investigate how the initial design affects the final generated skeleton layout. Three other different initial profiles are tested as shown in Fig. 5. It is found that all initial designs result in the circumferential bars, but the skeleton layout on the compressive side depends on whether holes are initially placed on the boundary. Besides, the optimization results present the size effect which means the final delivered geometric complexities depend on the initial

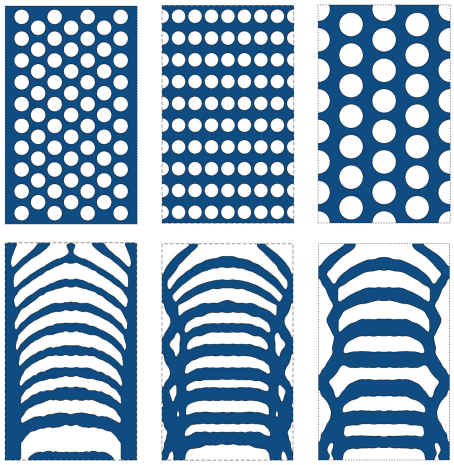

Fig. 5: Three different initial designs (the first row) and their corresponding optimization results (the second row).

hole density, which may inherently be related to the non-convexity of the displacement-oriented optimization problem. Based on these phenomena, we finally select the initial design as shown by state I in Fig. 4 which outperforms the three candidates in Fig. 5.

We further investigate how the optimized skeleton depends on the volume constraint. The volume fraction is increased from 0.3 to 0.7 with an interval of 0.1, and the associated optimized designs and their performance are compared as shown in Fig. 6. As the volume fraction increases from 0.3 to 0.5, the design produces enhanced bending benefiting from stronger constraining effect imposed by the hard material distributed on the compressive side. Thereafter, an evident decrease in bending motion is observed with the increasing volume fraction. On the one hand, the accumulation of material around the stripes suppresses the tensile deformation. On the other hand, more materials distributed on the compressive side increase the whole stiffness of the actuator. Thus, the volume fraction is set 0.5 for the final design.

V. Experiments and Applications

A. Material Selection and Actuator Fabrication

It can be inferred from dimensionless analysis that the performance of the actuator partially depends on the material modulus ratio of the skeleton to the soft rubber. A skeleton layer too soft cannot exert a constraining effect, while a skeleton layer too rigid would increase the overall actuator stiffness. Thus, there exists an optimal material ratio which can be roughly estimated by finite element analysis based on a selected skeleton layout, falling between 25 and 40. In consideration of the available materials off-the-shelf, we choose Dragon Skin 20 (Smooth-On, USA) as the soft rubber material whose viscosity, ductility and strength are satisfactory and HeiCast 8400 (Shore 90A, WeNext Technology, China) as the skeleton material. The ratio of their Young's modulus is around 35. The cylindrical shape soft layer is fabricated by injection molding. The material mixing and injection processes

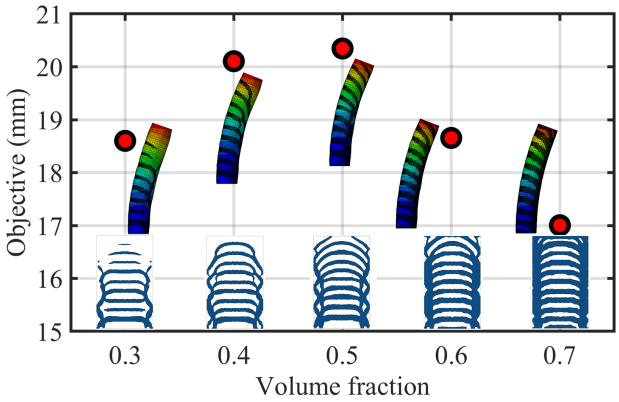

Fig. 6: The optimization solution depends on the volume fraction. The optimized designs and deformed shapes at 60 kPa are plotted as insets.

are performed simultaneously in a vacuum environment. The skeleton layer is fabricated by compound mold techniques. The fabricated parts as shown in Fig. 7(a) are assembled to build a soft bending actuator prototype.

B. Experiment Setup

The characterization of the actuator involves the control of pressure and the measurements of displacement and force. The whole experiment setup is shown in Fig. 7(b). The soft actuator is fixed to a rigid basement and is connected to an analog pneumatic close-loop controller (SMC, Japan). The motion of the actuator is tracked by a motion capture system (OptiTrack, USA). We use two phosphor markers [see Fig. 7(b)] adhering to the fingertip to capture the displacements. An S-beam load cell (ARIZON China) with customized fixture matching the shape of fingertip is deployed to record the contact force generated by the actuator upon pressurization.

C. Bending Actuator Characterization

Fig. 7(c) shows the free travel trajectory. The actuator prototype is pressurized at a speed of 4.8 kPa/s to simulate a quasi-static process. We repeat five loading circles in the pressure range of 0-120 kPa. The free motion exhibits excellent repeatability, as indicated by the narrow error bar in Fig. 7(c). The bending angle increases with the applied pressure, and reaches 73° under 120 kPa. A nonlinear finite element simulation is conducted which matches well with the trajectories in the range of 0-90 kPa with the maximal deviation less than 4.0%.

We also characterize the load capabilities of the actuator prototype by evaluating the blocking force. As shown in Fig. 7(d), the blocking force increases with the applied pressure, peaking at 2.05 N under 120 kPa. It is noted that, although the power requirement is not directly included in the design objective of the optimization model (9), the skeleton still attains considerable stiffness which leads to good load capabilities. The inner soft rubber as the non-design domain owns considerable stiffness to withstand the gravity, and thus the skeleton layer must be stiffer to dominate the bending motion, which leads to the remarkable load capability of the actuator.

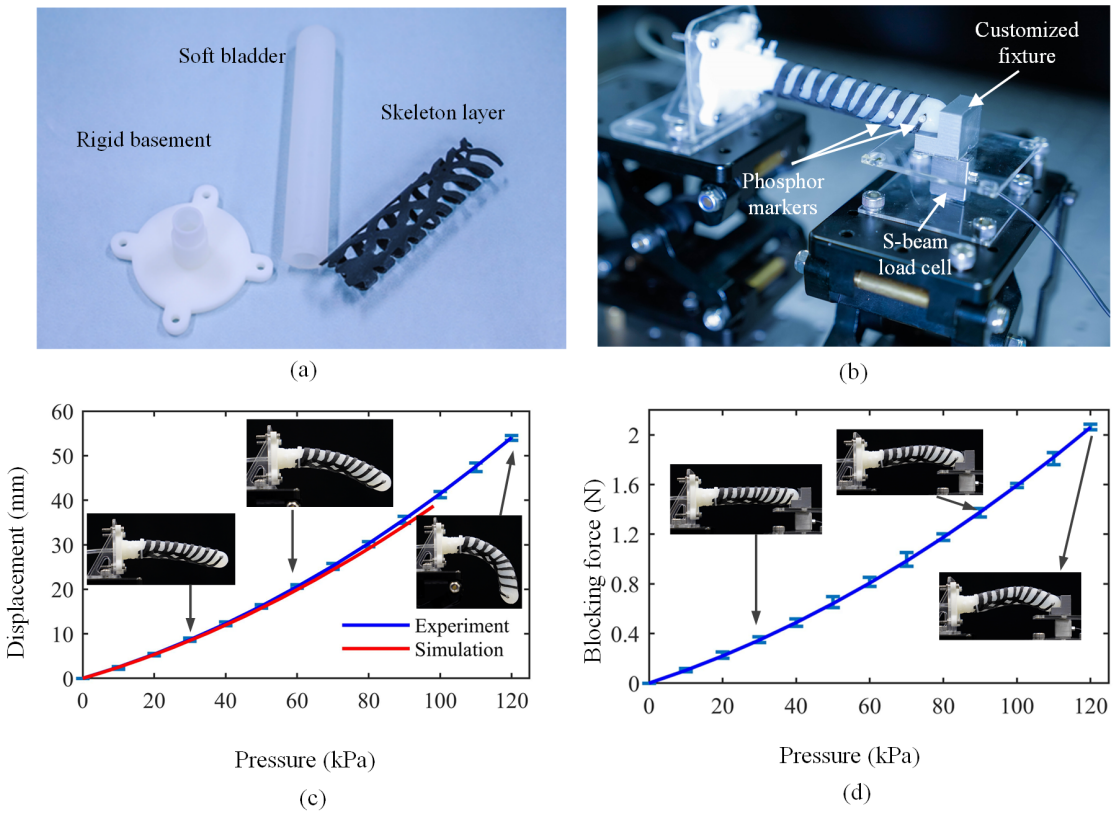

Fig. 7: Experiment results: (a) components; (b) the bending actuator prototype; (c) free motion and (d) blocking force tests.

VI. Extension and Discussion

A. Extension

To demonstrate the generality of the design method, we further extend the cases studies to more types of motions and more complex design domain. Bending and twisting motions of a cone-shaped actuator are investigated by firstly constructing geometry and velocity mappings from the regular 2D design domain to the 3D cone surface according to (3), and by secondly modifying the design objective to capture the desired motion. It is worth noting that, different from cylindrical surface, the geometry mapping is not isometric and the design velocity mapping is not uniform. The upper base radius of the cone is 5.57 mm, and the bottom radius is 7.95 mm. The other parameters and the boundary conditions keep unchanged with the case in Sec. IV.

Fig. 8 shows the optimized design of the cone-shaped actuator toward bending and twisting motions, and the simulation and experimental results. Specifically, for bending motion, the design pattern is similar to the case in Sec. IV except that the geometric features vary in size. For twisting motion, the design objective is to maximize the tangential displacements of points on the edge, and the optimized solution generates chiral patterns which are also physically reasonable. The experiment shows that the actuator twists by 143° under 60 kPa. The smoothness of the skeleton pattern is again guaranteed by the domain continuity operation. Here, it is emphasized that our design method provides a rational and quantitative guidance for design of soft bodied actuators and robots.

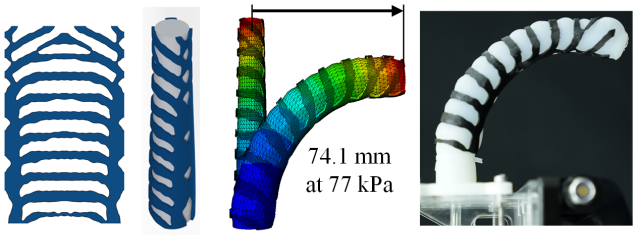

(a) Bending design of a cone-shaped actuator

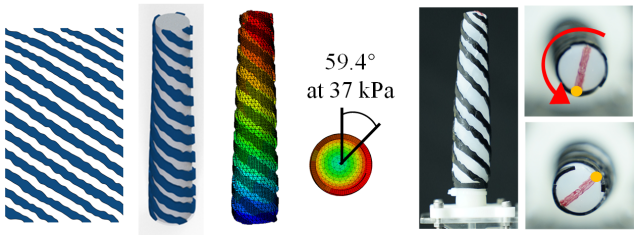

(b) Twisting design of a cone-shaped actuator

Fig. 8: Skeleton optimization for cone-shaped actuator's (a) bending or (b) twisting motion. From left to right: the skeleton layout, simulation result and experimental result.

B. Discussion

The design space can be further explored. For example, the thickness dimension has been designed to tune the spatially-varying bending abilities toward desired deformations [24]. The skeleton layout plays an important role in modulating

the global motion behavior, while its non-uniform thickness is expected to exert major impact on local deformations. In this work, we only carry out surface design because we focus more on the global motion and the thickness variations may cause convergence issues in finite element analysis for large deformation. Nevertheless, we believe that, the incorporation of thickness will further explore the design space to deliver better design, and may become necessary to more complicated design problems such as shape-matching in which many local features are pursued. It is also noted that, although only bending and twisting deformations are investigated, the proposed method is readily applicable to more complicated desired motions by directly modifying the design objective.

When dealing with general free-form surfaces, the key is still to establish the geometric mapping and inverse design velocity mapping, except that the mappings may not be constructed explicitly but numerically. The conformal mapping theory can be combined with topology optimization theories to recast the manifold embedded in the 3D space as a 2D topology optimization problem in the Euclidean space. Ye *et al.* provided a unified level-set-based computational framework for the generative design of free-form structures by conformally mapping the manifolds onto a 2D rectangle domain where the level set function is defined [25]. This operation allows for the convenient use of conventional computational schemes for level set methods by solving the modified Hamilton-Jacobi equation.

VII. Conclusion

We build an actuator design paradigm by attaching a stiffer material layer as skeleton to softer inflated rubber, and develop a topology optimization based design framework to automatically generate the skeleton layout that leads the actuator to achieve desired motions such as bending and twisting. To capture large deformation that typically occurs in soft robots, our optimizer incorporates the geometric and material nonlinearities, and the generated design contains reliable and explainable structural features that provide new insights for designers. The simulation and experiment results agree well in both linear and nonlinear regions, and validate that our designed actuator achieves remarkable bending motions with considerable force capabilities. We further investigate the design of cone-shaped actuators toward bending and twisting motions to demonstrate the generality of the proposed method. In the future, we hope to further generalize the design methodology to free-form surfaces for creating soft-bodied robots of customizable shapes capable of undergoing more complex motion behaviors.

References

[1] F. Chen and M. Y. Wang, "Design optimization of soft robots: A review of the state of the art," *IEEE Robotics and Automation Magazine*, vol. 27, no. 4, pp. 27–43, 2020.

[2] M. Schaffner, J. A. Faber, L. Pianegonda, P. A. Rühs, F. Coulter, and A. R. Studart, "3d printing of robotic soft actuators with programmable bioinspired architectures," *Nature communications*, vol. 9, no. 1, pp. 1–9, 2018.

[3] K. Kumar, J. Liu, C. Christianson, M. Ali, M. T. Tolley, J. Aizenberg, D. E. Ingber, J. C. Weaver, and K. Bertoldi, "A biologically inspired, functionally graded end effector for soft robotics applications," *Soft robotics*, vol. 4, no. 4, pp. 317–323, 2017.

[4] N. W. Bartlett, M. T. Tolley, J. T. Overvelde, J. C. Weaver, B. Mosadegh, K. Bertoldi, G. M. Whitesides, and R. J. Wood, "A 3d-printed, functionally graded soft robot powered by combustion," *Science*, vol. 349, no. 6244, pp. 161–165, 2015.

[5] P. Polygerinos, Z. Wang, J. T. Overvelde, K. C. Galloway, R. J. Wood, K. Bertoldi, and C. J. Walsh, "Modeling of soft fiber-reinforced bending actuators," *IEEE Transactions on Robotics*, vol. 31, no. 3, pp. 778–789, 2015.

[6] J. Bishop-Moser and S. Kota, "Design and modeling of generalized fiber-reinforced pneumatic soft actuators," *IEEE Transactions on Robotics*, vol. 31, no. 3, pp. 536–545, 2015.

[7] J. Zou, M. Feng, N. Ding, P. Yan, H. Xu, D. Yang, N. X. Fang, G. Gu, and X. Zhu, "Muscle-fiber array inspired, multiple-mode, pneumatic artificial muscles through planar design and one-step rolling fabrication," *National Science Review*, 2021.

[8] F. Connolly, C. J. Walsh, and K. Bertoldi, "Automatic design of fiber-reinforced soft actuators for trajectory matching," *Proceedings of the National Academy of Sciences*, vol. 114, no. 1, pp. 51–56, 2017.

[9] J. Hiller and H. Lipson, "Automatic design and manufacture of soft robots," *IEEE Transactions on Robotics*, vol. 28, no. 2, pp. 457–466, 2012.

[10] M. Skouras, B. Thomaszewski, S. Coros, B. Bickel, and M. Gross, "Computational design of actuated deformable characters," *ACM Transactions on Graphics (TOG)*, vol. 32, no. 4, pp. 1–10, 2013.

[11] F. Chen, W. Xu, H. Zhang, Y. Wang, J. Cao, M. Y. Wang, H. Ren, J. Zhu, and Y. Zhang, "Topology optimized design, fabrication, and characterization of a soft cable-driven gripper," *IEEE Robotics and Automation Letters*, vol. 3, no. 3, pp. 2463–2470, 2018.

[12] F. Chen, K. Liu, Y. Wang, J. Zou, G. Gu, and X. Zhu, "Automatic design of soft dielectric elastomer actuators with optimal spatial electric fields," *IEEE Transactions on Robotics*, vol. 35, no. 5, pp. 1150–1165, 2019.

[13] J. Tian, X. Zhao, X. D. Gu, and S. Chen, "Designing ferromagnetic soft robots (ferrosoro) with level-set-based multiphysics topology optimization," in *2020 IEEE International Conference on Robotics and Automation (ICRA)*. IEEE, 2020, pp. 10 067–10 074.

[14] L.-K. Ma, Y. Zhang, Y. Liu, K. Zhou, and X. Tong, "Computational design and fabrication of soft pneumatic objects with desired deformations," *ACM Transactions on Graphics (TOG)*, vol. 36, no. 6, pp. 1–12, 2017.

[15] Y. Chen, Z. Xia, and Q. Zhao, "Optimal design of soft pneumatic bending actuators subjected to design-dependent pressure loads," *IEEE/ASME Transactions on Mechatronics*, vol. 24, no. 6, pp. 2873–2884, 2019.

[16] B. Mosadegh, P. Polygerinos, C. Keplinger, S. Wennstedt, R. F. Shepherd, U. Gupta, J. Shim, K. Bertoldi, C. J. Walsh, and G. M. Whitesides, "Pneumatic networks for soft robotics that actuate rapidly," *Advanced Functional Materials*, vol. 24, no. 15, pp. 2163–2170, 2014.

[17] H. Zhang, A. S. Kumar, F. Chen, J. Y. Fuh, and M. Y. Wang, "Topology optimized multimaterial soft fingers for applications on grippers, rehabilitation, and artificial hands," *IEEE/ASME Transactions on Mechatronics*, vol. 24, no. 1, pp. 120–131, 2019.

[18] S. Osher and J. A. Sethian, "Fronts propagating with curvature-dependent speed: algorithms based on hamilton-jacobi formulations," *Journal of computational physics*, vol. 79, no. 1, pp. 12–49, 1988.

[19] M. Y. Wang, X. Wang, and D. Guo, "A level set method for structural topology optimization," *Computer methods in applied mechanics and engineering*, vol. 192, no. 1, pp. 227–246, 2003.

[20] M. Y. Wang, H. Zong, Q. Ma, Y. Tian, and M. Zhou, "Cellular level set in B-splines (CLIBS): A method for modeling and topology optimization of cellular structures," *Computer Methods in Applied Mechanics and Engineering*, vol. 349, pp. 378 – 404, 2019.

[21] R. Rivlin, "Large elastic deformations of isotropic materials iv. further developments of the general theory," *Philosophical Transactions of the Royal Society of London. Series A, Mathematical and Physical Sciences*, vol. 241, no. 835, pp. 379–397, 1948.

[22] F. Chen, Y. Wang, M. Y. Wang, and Y. Zhang, "Topology optimization of hyperelastic structures using a level set method," *Journal of Computational Physics*, vol. 351, pp. 437–454, 2017.

[23] Q. Pan, S. Chen, F. Chen, and X. Zhu, "Programmable soft bending actuators with auxetic metamaterials," *Science China Technological Sciences*, vol. 63, no. 12, pp. 2518–2526, 2020.

[24] X. T. Zhang, X. Y. Le, Z. H. Wu, E. Whiting, and C. C. L. Wang, "Data-driven bending elasticity design by shell thickness," *Computer Graphics Forum*, vol. 35, no. 5, pp. 157–166, 2016.

[25] Q. Ye, Y. Guo, S. Chen, N. Lei, and X. D. Gu, "Topology optimization of conformal structures on manifolds using extended level set methods (x-lsm) and conformal geometry theory," *Computer Methods in Applied Mechanics and Engineering*, vol. 344, pp. 164–185, 2019.

Shitong Chen received the B.E. degree in aircraft design engineering from Xi'an Jiaotong University, Xi'an, China, in 2018. He is currently working toward the Ph.D. degree in mechanical engineering at Shanghai Jiao Tong University, Shanghai, China.

His research interests include computational design of soft robots.

Feifei Chen (Member, IEEE) received the B.E. degree in mechanical engineering from University of Science and Technology of China in 2013, and Ph.D. degree in mechanical engineering from National University of Singapore in 2018. He joined Shanghai Jiao Tong University in 2018 and currently is an Associate Professor (tenure-track) with the School of Mechanical Engineering.

His research interests have been focused on design thoery and methods for soft robots.

Zizheng Cao is currently working toward the B.E. degree in mechanical engineering at Shanghai Jiao Tong University, Shanghai, China.

His research interests include design, manufacture, and simulation of soft robots.

Yusheng Wang is currently working toward the B.E. degree in mechanical engineering at Shanghai Jiao Tong University, Shanghai, China.

His research interests include computational mechanics, robotics and smart materials.

Yunpeng Miao received the B.E. degree in mechanical engineering from East China University of Science and Technology, Shanghai, China, in 2019. He is currently working toward the M.S. degree in mechanical engineering at Shanghai Jiao Tong University, Shanghai, China.

His research interests include geometric modeling and optimization of soft robots.

Guoying Gu (Member, IEEE) received the B.E. degree (with honors) in electronic science and technology, and the Ph.D. degree (with honors) in mechatronic engineering from Shanghai Jiao Tong University, Shanghai, China, in 2006 and 2012, respectively. Since October 2012, Dr. Gu has worked at Shanghai Jiao Tong University, where he is currently appointed as a Professor of School of Mechanical Engineering. He was a Humboldt Fellow with University of Oldenburg, Germany. He was a Visiting Scholar at Massachusetts Institute of Technology, National University of Singapore and Concordia University. His research interests include soft robotics, bioinspired and wearable robots, smart materials sensing, actuation and motion control. He is the author or co-author of over 90 publications, which have appeared in Science Robotics, Science Advances, IEEE/ASME Trans., Advanced Functional Materials, Soft Robotics, etc., as book chapters and in conference proceedings.

Dr. Gu received the National Science Fund for Distinguished Young Scholars in 2020. Now he serves as Associate Editor of IEEE Transactions on Robotics and IEEE Robotics and Automation Letters. He has also served for several journals as Editorial Board Member, Topic Editor, or Guest Editor, and several international conferences/symposiums as Chair, Co-Chair, Associate Editor or Program Committee Member.

Xiangyang Zhu (Member, IEEE) received the B.S. degree in automatic control from Nanjing Institute of Technology, Nanjing, China, in 1985, the M.Phil. degree in instrumentation engineering and the Ph.D. degree in control engineering, both from Southeast University, Nanjing, China, in 1989 and 1992, respectively. From 1993 to 1994, he was a postdoctoral research fellow with Huazhong University of Science and Technology, Wuhan, China. He joined the Department of Mechanical Engineering, Southeast University, as an associate professor in 1995. Since June 2002, he has been with the School of Mechanical Engineering, Shanghai Jiao Tong University, Shanghai, China, where he is currently a chair professor and the director of the Robotics Institute. His research interests include robotic manipulation planning, neuro-interfacing and neuro-prosthetics, and soft robotics. He has published more than 200 papers in international journals and conference proceedings.

Dr. Zhu has received a number of awards including the National Science Fund for Distinguished Young Scholars from NSFC in 2005, and the Cheung Kong Distinguished Professorship from the Ministry of Education in 2007. He currently serves on the editorial board of the IEEE Transactions on Cybernetics and Bio-design and Manufacturing.